Geophysical Research Letters

RESEARCH LETTER
10.1029/2021GL096933

Key Points:

- Using a stream-power erosion model with locally calibrated coefficients we calculated across-fault gully incision ages
- Constant sinistral slip of 0.5 ± 0.1 mm/yr since 52 ± 4 ka is calculated for the eastern termination of the Altyn Tagh Fault
- Our results are consistent with episodic rather than continuous growth of the Tibetan plateau northeastwards into central Asia

Supporting Information:

Supporting Information may be found in the online version of this article.

Correspondence to:

N. Wieler,
wielern@gmail.com

Citation:

Wieler, N., Mushkin, A., Zhang, H., Sagy, A., Porat, N., Shmilovitz, Y., et al. (2022). Geomorphic dating of across-fault gully incision reveals time-invariant late Quaternary slip-rates at the eastern termination of the Altyn Tagh Fault. *Geophysical Research Letters*, *49*, e2021GL096933. https://doi.org/10.1029/2021GL096933

Received 22 NOV 2021
Accepted 11 APR 2022

Geomorphic Dating of Across-Fault Gully Incision Reveals Time-Invariant Late Quaternary Slip-Rates at the Eastern Termination of the Altyn Tagh Fault

Nimrod Wieler[1], Amit Mushkin[1], Huiping Zhang[2], Amir Sagy[1], Naomi Porat[1], Yuval Shmilovitz[1,3], Zhikun Ren[2], Feipeng Huang[2], Pilong Shi[4], Jinrui Liu[2], and Eitan Shelef[5]

[1]Geological Survey of Israel, Jerusalem, Israel, [2]State Key Laboratory of Earthquake Dynamics, Institute of Geology, China Earthquake Administration, Beijing, China, [3]Institute of Earth Sciences, Hebrew University of Jerusalem, Jerusalem, Israel, [4]Institute of Remote Sensing and Digital Earth, Chinese Academy of Sciences, Beijing, China, [5]Department of Geology and Environmental Science, University of Pittsburgh, Pittsburgh, PA, USA

Abstract Interpretation of fault slip-rates inferred from tectonically offset fluvial landforms is often limited by uncertainties associated with difficulties to explicitly date fluvial incision across the fault. Here, we employed morphology-based modeling to ameliorate this universal dating limitation for gullies that were differentially offset in a sinistral sense across the Altyn Tagh Fault near its eastern termination at ~97°E. Using a stream-power erosion model with locally calibrated coefficients we calculated across-fault gully incision ages that decrease with offset magnitude, are up to threefold younger than the age of the terrace they incised and all-together point toward time-invariant slip. Luminescence dating of offset alluvial terraces at the same site suggests constant sinistral slip at 0.5 ± 0.1 mm/yr since 52 ± 4 ka. Our results suggest that the most juvenile phase of northeastward Pleistocene expansion of the Tibetan Plateau into previously stable parts of central Asia is marked by constant late Quaternary deformation rates.

Plain Language Summary Horizontally deflected streams in tectonically active landscapes are often used by geoscientists to infer fault slip-rates over geologic timescales. Our results demonstrate the potentially high degree of uncertainty that may be associated with this approach because incision itself is hard to date and age control for the deflected streams is conventionally indirectly obtained from dating the surface they incise and/or sediments they accumulate. Here, we applied morphology-based modeling of fluvial incision to address this dating limitation for deflected streams near the eastern termination of the Altyn Tagh Fault in central Asia. Explicit dating of fluvial incision revealed across-fault incision ages that were threefold younger than the age of the alluvial terrace incised and constant horizontal slip-rates that were similar to longer-term late Quaternary slip-rates we obtained at the same site using offset terrace boundaries and luminescence dating for age control. Our results suggest that the late Pleistocene expansion phase of the Tibetan plateau northeastwards into central Asia is characterized by constant rates of deformation during the late Quaternary.

1. Introduction

Geologic features offset across discrete fault lineaments are routinely utilized to determine tectonic slip-rates over timescales of hundreds to millions of years (Burbank & Anderson, 2011). Such "geologic slip-rates" are conventionally obtained by dividing measured offset distance by estimated offset duration, which is usually inferred through dating of the offset marker. Ambiguities in the reconstruction of offset features together with complications in determining their age are the most common sources for measurement uncertainties in calculated geologic slip-rates (Cowgill, 2007; Reitman et al., 2019; Zechar & Frankel, 2009; Zielke et al., 2015).

In the prevalent case of strike-slip faulting rates inferred from fluvially incised landforms, such as offset channels and terrace risers, the lack of a systematic method to explicitly date the across-fault incision of such landforms presents an additional component of uncertainty, because their age is typically constrained to be younger than the age of the strata they incise and/or older than the age of post-incision deposits they accommodate (Figure 1). However, because erosional landforms are inherently younger than the deposit they incise and are necessarily older than the sediments they accumulate, it is broadly recognized that fault slip-rates based on such minimum/maximum age control intrinsically under- or over-estimate the actual rate of tectonic slip, respectively (D'Arcy et al., 2019; Duvall & Tucker, 2015; Harkins & Kirby, 2008; Figure 1).

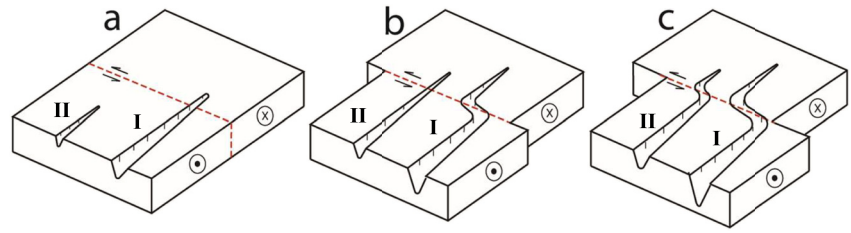

Figure 1. Illustration of fluvial incision through time across a strike-slip fault. Channels may start recording tectonic offsets after they effectively incise across the fault. Adjacent channels that incise the same stratum and cross the same fault line can record variable offset magnitudes depending on when across-fault incision occurred. (a) Channel *I* is incised across a fault while channel *II* is not. (b) Fault slip between the time described by panel (a and b) offset channel *I* while channel *II* only recently incised across the fault and therefore is not yet offset. (c) Continued fault-slip offsets both channels. Accumulated offset recorded by channel *I* is larger than that of adjacent channel *II*. Explicit dating of across-fault incision is required to accurately infer fault slip-rates from such offset features.

Studies of secular variability in Quaternary-scale fault slip-rates are particularly impacted by this difficulty to obtain tightly constrained across-fault incision ages because uncertainties from multiple slip-rate measurements become compounded and the resulting uncertainty may conceal secular changes in slip-rate (e.g., Gold et al., 2011). Thus, although studies of long-term secular variability in geologic slip-rates of strike-slip faults have proven to be instrumental for understanding fault evolution (Bennett et al., 2004; Dolan et al., 2016; Gold et al., 2017; Ludwig et al., 2010)—they have remained universally restricted to only a handful of cases due, in large part, to the fundamental limitation of explicitly dating across-fault fluvial incision. Here, we developed a morphology-based modeling approach that addresses this dating limitation in the case of channel incision into abandoned alluvial surfaces and apply it to examine the secular behavior of late Quaternary slip-rates near the eastern termination of the Altyn Tagh Fault (ATF) in central Asia (Figure 2).

2. Geologic Background and Methods

2.1. The Eastern Termination of the ATF

The possibility of secular variability in slip-rates across the ATF has focused broad attention over recent decades (Chen et al., 2012; Cowgill, 2007; Cowgill et al., 2009; Elliott et al., 2015; Mériaux et al., 2005, 2012; Peltzer et al., 1989; Washburn et al., 2001; Xu, 2005) due to the ATF's role as the northern boundary of the Tibetan Plateau (Tapponnier & Molnar, 1977) and the ongoing debate regarding crustal deformation mechanisms in central Asia (Tapponnier, 2001; Zhang et al., 2004). Ultimately however, secular variability in the ATF's crustal velocity has been shown to be less likely as both geologic slip-rates during the last ~20 ka and geodetic measurements from recent decades reveal comparable sinistral slip-rates of 8–12 mm/yr across the central segment of the fault between 85° and 93°E (Chen et al., 2012; Cowgill et al., 2009; Gold et al., 2011, 2009; Washburn et al., 2001). Eastwards from ~93°E slip-rates gradually decrease down to zero velocity near ~97°E (Liu et al., 2020; Meyer et al., 1996; Xu, 2005; Zhang et al., 2007), where the ATF terminates within the Yumen Basin (Xiao et al., 2015; Zhang et al., 2020; Figure 2).

The gradual decrease in the ATF's sinistral slip-rates east of 93°E and the mid-continental termination of the fault are associated with gradual transfer of sinistral shear onto a sequence of oblique SE striking Tertiary thrust belts that occur south of the ATF within the Tibetan Plateau (He et al., 2013; Kang et al., 2020; Liang et al., 2013; Zheng et al., 2013; Figure 2). Initiation of faulting on these thrust belts becomes younger toward the east (Zheng et al., 2013) and together with the eastward propagation of the ATF (Allen et al., 2017; Yin et al., 2002; Zhang et al., 2020), they manifest the northeastwards growth of the Tibetan Plateau into central Asia (Hetzel, 2013; Hetzel et al., 2002; Tapponnier, 2001). In this context, the Pleistocene initiation of the Yumen Basin thrusts at ~2 Ma (Zheng et al., 2013), is commonly regarded to be the most juvenile expression of NE shear propagation of the Tibetan Plateau into the stable Gobi-Alashan block (Su et al., 2019; Zheng et al., 2013).

The eastwards Pleistocene propagation of the ATF into the Yumen Basin (Allen et al., 2017; Yin et al., 2002; Zhang et al., 2020) requires secular variability in lateral slip-rates at a fixed reference point along the ATF's Yumen segment as slip-rates had to increase thereafter the fault tip propagated eastwards beyond this point

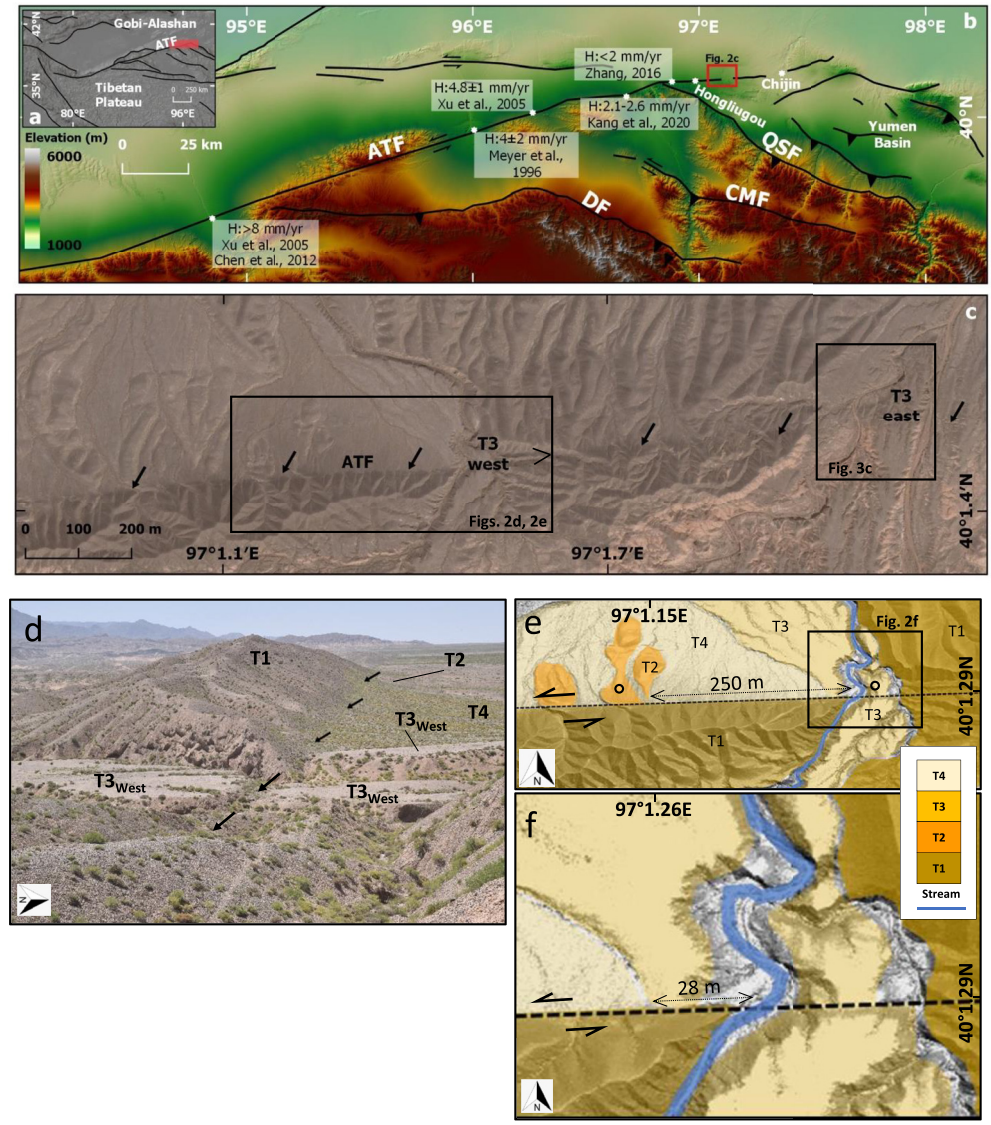

Figure 2. The Chijin site at the northern boundary of the Yumen Basin. (a, b) The Altyn Tagh Fault; Changma Fault (CMF); Daxue Fault (DF); Qilian Shan Fault (QSF) and major regional structures superimposed on topography (SRTM 90 m/pixel) at the northeastern edge of the Tibetan Plateau. (c) Google Earth image of the Chijin site. The Altyn Tagh Fault (ATF) (highlighted with black arrows) cuts through the sequence of Quaternary alluvial terraces. (d) Field photo looking westwards onto $T3_W$ and the other alluvial terraces at the site (vantage point marked with open v shape in (c)). Note the well-preserved flat desert pavement surface of $T3_W$ on both sides of the fault. (e, f) Chronostratigraphic map of the Chijin site showing the sinistral offsets of T2 and $T3_W$. Open black circles mark the sampling locations for luminescence dating.

(Wesnousky, 2006). However, similar geologic Holocene slip-rates and modern geodetic velocities measured across the Yumen segment of the ATF (Kang et al., 2020; Li et al., 2018; Zhang et al., 2007) argue against secular variability in slip near the ATF's tip during this period. Accordingly, we focused herein on longer-term secular variability in the ATF's lateral slip-rates at a field site close to the ATF tip within the Yumen basin. Gradually increasing Pleistocene slip-rates near the ATF's terminus is suggested to be consistent with a gradual shear-propagation model for the Tibetan Plateau (e.g., Molnar & Dayem, 2010; Zhang et al., 2004), whereas prolonged periods of time-invariant slip-rates would point toward a "step-wise" episodic shear-propagation model (Jiang & Li, 2014; Tapponnier, 2001), in which shear expansion is likely associated with discrete episodes of slip acceleration near the fault terminus.

2.2. The Chijin Site

The decline of lateral slip-rates east of 93°E (Figure 2) precludes inferences of secular variability in fault activity rates by amalgamation and comparison of geologic slip-rates obtained at multiple sites (Gold et al., 2017) and instead requires adequate dating of multiple generations of offsets markers at a single location (Ludwig et al., 2010). We, therefore, focused on a unique site along the northern border of the Yumen Basin, approximately 30 km west of Chijin (Figure 2b), where multiple generations of abandoned alluvial terraces and three fluvial channels are differentially offset in a sinistral sense across the same segment of the ATF by distances ranging from ∼250 to 8 m (Figures 2 and 3). To calculate slip-rates from the offset terraces we applied luminescence dating for age control (Section 3 below) and for slip-rates inferred from the offset channels we developed a locally calibrated geomorphic modeling approach to explicitly determine the timing at which each of offset channel incised across the fault (Section 4 below).

2.3. Methods

Luminescence dating was applied to obtain age control for the alluvial-terrace sequence at the Chijin site (Supporting Information S1). Sampling of the terraces deposits was carried out using an aluminum tube inserted into sand lenses exposed in cut bank exposures. Samples were processed and measured at the Geological Survey of Israel following Faershtein et al. (2016). Dose rates were calculated from concentrations of U, Th, and K in the samples, measured using inductively coupled plasma mass spectrometry (ICP-MS; U and Th) or ICP optical emission spectrometry (ICP-OES; K) and cosmic doses were calculated from burial depths (Prescott & Hutton, 1994). Equivalent doses (De) were measured using a modified single aliquot regenerative dose protocol (Murray & Wintle, 2000). All luminescence measurements were carried out using Riso TL/OSL DA-12 or DA-20 readers equipped with blue diodes (power on sample of 37 mW). Age calculations are based on the central age model (Galbraith et al., 1999) that is designed to identify the central tendency in a dose distribution (Supporting Information S1).

Drone-based images acquired at the Chijin site were processed with the AGISOFT software package (www.agisoft.com) to produce a 5 cm/pixel DEM (Figure 3; Supporting Information S1). Topographic data extracted from the DEM were used as input for the geomorphic model used to reconstruct the time-dependent incision of the offset channels.

3. Luminescence Ages and Slip-Rates Calculations for Offset Terraces

The main branch of the ATF strikes ∼ E-W across the Chijin site where it is localized within a 1.5-m-wide fault-zone that cuts through a sequence of four abandoned alluvial-fan units that overlie fluvio-Lacustrine Neogene red-beds (Wang et al., 2016; Figure 2). These morphostratigraphic terraces (T1–T4) were mapped in the field based on their relative height above the active channel and neighboring terraces, as well as sedimentological characteristics such as clast assemblage, and soil profile and pavement maturity. T1 is the oldest unit and T4 is the youngest. A saturated (i.e., minimum) luminescence age obtained for unit T2 indicates its deposition prior to 176 ± 12 ka and ages of 115 ± 21 and 52 ± 4 ka obtained near the base and top of unit T3, respectively, place T3 within the late Pleistocene (Figures 2 and 3).

Remnants of unit T2 deposits preserved just north of the fault trace record a sinistral offset of at least 250 ± 10 m across the ATF (Figure 2). Together with the minimum age for T2 (i.e., >176 ± 12 ka) we calculated a maximum time-averaged slip-rate of 1.4 ± 0.2 mm/yr for T2. Unit T3 is better preserved at the Chijin site and is characterized by a 1–3 m thick section of moderately consolidated, approximately horizontally layered, sub-rounded alluvial pebbles and intercalated sand lenses all capped by a well-developed, mature desert-pavement surface (Figures 2 and 3). At the two locations where intact T3 pavement surfaces overlay the ATF, they record similar vertical offsets of 1.2 ± 0.4 m (Figure in Supporting Information S1). A sinistral offset of 28 ± 2 m is recorded by the western T3 terrace ("$T3_W$"; Figure 2). Assuming 52 ± 4 ka for T3 abandonment we calculated a time-averaged horizontal slip of 0.54 ± 0.08 mm/yr since terrace abandonment (Figure 4) accompanied by a minor vertical slip-component of 0.02 ± 0.01 mm/yr.

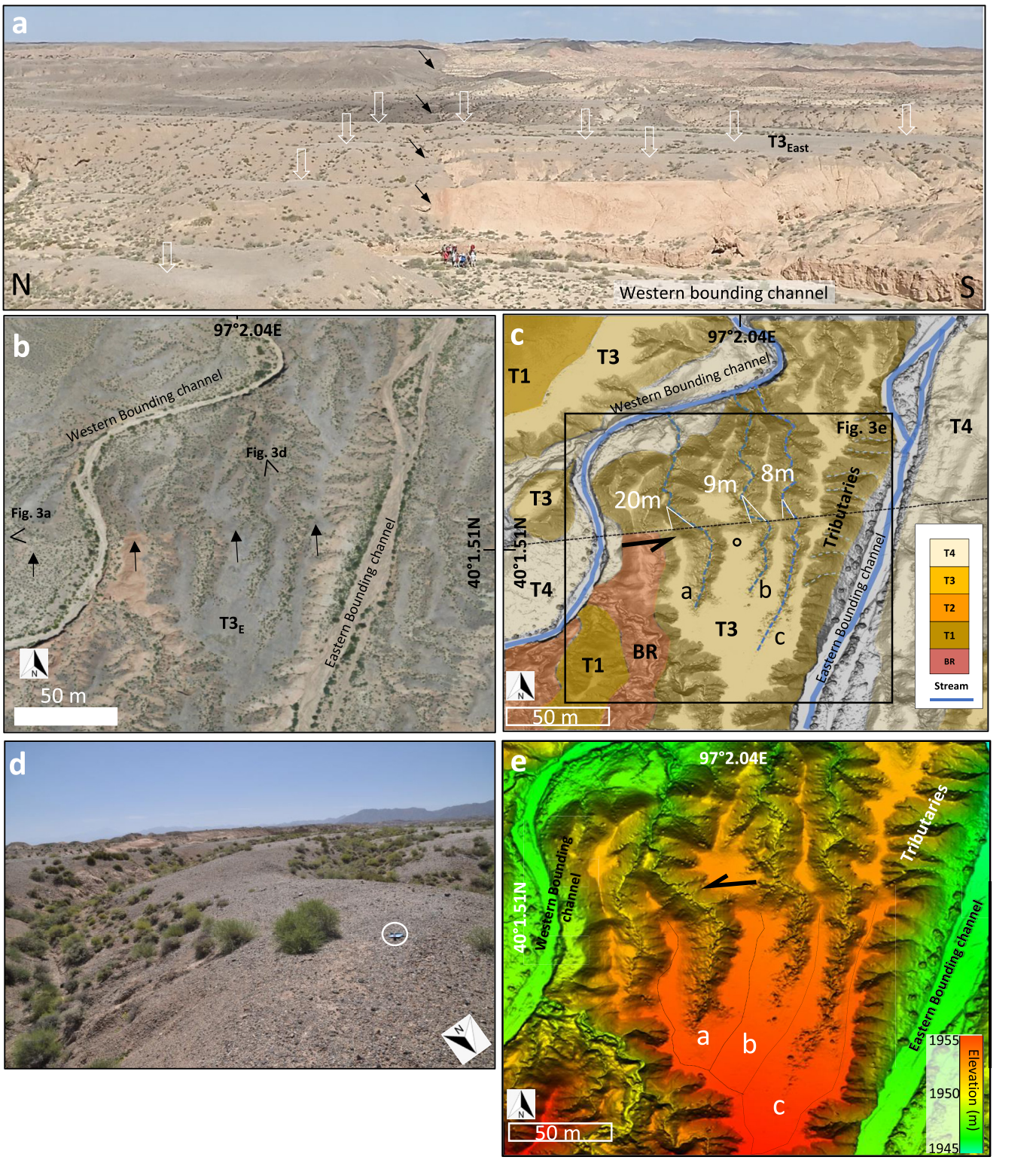

Figure 3. Terrace $T3_W$ and offset gullies a–c. (a) Field photo of T3w and the ATF (black arrows). White arrows highlight well-preserved flat desert-pavement surfaces of T3w on both sides of the fault. People for scale in the foreground. (b) Orthophoto (5 cm/pixel) for T3w. Black arrows mark the ATF. Open v shape marks the vantage points of field photos in (a and d), respectively. (c) Morphostratigraphic map of the same areas as (b). Black circle marks location of luminescence sample collection. BR stands for bedrock (d) photograph looking southwards onto offset gullies b and c and the surrounding preserved desert pavement surfaces (hammer for scale, 30 cm long, marked with white circle). (e) Shaded relief image for $T3_E$ and offset gullies a–c produced from a 5 cm/pixel DEM. Dotted black lines mark the drainage boundaries for each gully above the fault line.

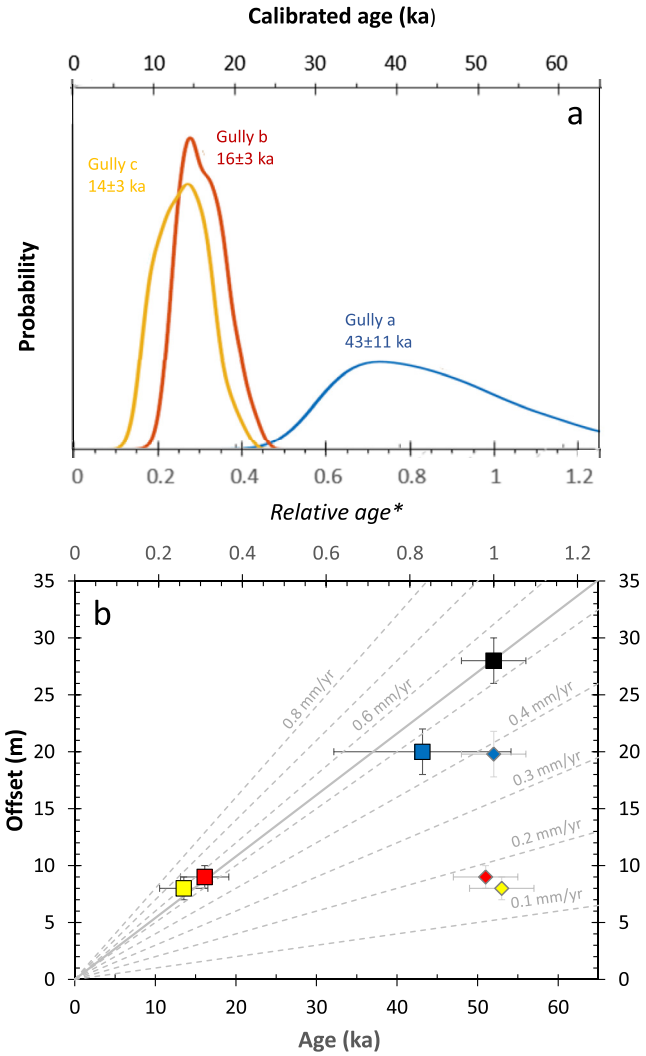

Figure 4. Across-fault incision ages for gullies a–c and inferred slip-rates. (a) Model-result for the timing of across-fault incision for gullies offset a–c. Primary (bottom) *x*-axis are ages relative to the age of T3 and secondary (top) *x*-axis is for calibrated age results assuming 52 ka for T3. (b) Inferred slip-rates assuming calibrated ages plotted on the primary *x*-axis and relative ages on the secondary *x*-axis using the same color scheme as in *A* for gully incision ages (color squares). Black square is for $T3_W$. Dashed lines mark calculated slip-rates of 0.1–0.8 mm/yr. Colored diamonds (slightly offset along the *x*-axis for clarity) mark erroneous slip-rates that would theoretically be inferred by using the age of T3 for offset duration for the offset of gullies a–c.

4. Across-Fault Incision Ages and Slip-Rate Calculations for Offset Gullies

The lateral offset of the eastern T3 terrace ("$T3_E$") could not be determined as it is elevated 8–9 m above two north-flowing bounding channels that have eroded its original depositional boundaries (Figure 3). However, three channels that internally drain $T3_E$ into its western bounding channel are sinistrally offset by the ATF. These relatively small channels termed herein as gullies a, b, and c, are unique in that they record variable lateral offsets of 20 ± 1.5, 9 ± 2, and 8 ± 2 m, respectively, while maintaining hydraulic connectivity between their above and below-fault sections. The proximity of gullies a-c within 50 m of each other precludes a tectonic origin for the two-fold difference in their sinistral offset and suggests that asynchronous across-fault incision is the more likely explanation (Figure 1). Slip-rate calculations for gullies a-c therefore require explicit dating of the across-fault incision of each gully separately.

Morphology-based dating through landform evolution modeling has been previously applied in various geological settings. For example, fault-scarp morphology was used to constrain timing of fault activity assuming that post-faulting degradation of the fault-scarp morphology can be modeled as a time-dependent diffusion process (e.g., Andrews & Hanks, 1985; Enzel et al., 1996; Hilley et al., 2010). Under similar assumptions, the age of abandoned alluvial terraces was estimated by examining profiles of gully banks (Hsu & Pelletier, 2004; Xu et al., 2021) or the surface roughness of such terraces (Frankel & Dolan, 2007). At larger spatial scales the timing and magnitude of changes in tectonic uplift rates was estimated based on the geometry of longitudinal channel profiles (Fox et al., 2014; Goren, Willett, et al., 2014) assuming that fluvial erosion rate can be modeled, via the stream-power law, as a function of drainage area and slope (Goren, Fox, et al., 2014; Howard & Kerby, 1983; Whipple & Tucker, 1999). In the present study, we use a similar assumption to date the fluvial incision of gullies a–c across the surface of unit $T3_E$ and into its N-S bounding channels. Building on: (a) the moderate cementation of the $T3_E$ alluvium, which supports cut-bank morphologies; (b) the typical v-shaped cross-section of the gullies that incise it, and (c) the thin to non-existent accumulation of post-incision deposits within the gullies (Figure 3)—we assume that the $T3_E$ deposits can be regarded as a "highly erodible bedrock" and that the incision rate (dz/dt) of these gullies into $T3_E$ can be modeled as a detachment limited process (e.g., Howard, 1994; Whipple & Tucker, 1999), such that:

$$dz/dt = KA^mS^n \quad (1)$$

where dz/dt [L/t] is incision rate, and A [L^2] and S are drainage area and slope, respectively. K [$L^{(1-2m)}/t$] is an erodibility coefficient that accounts for the effects of climate, lithology, and catchment geometry, and the exponents m and n indicate that incision rate can vary nonlinearly with A and S (Dietrich et al., 2003; Seidl & Dietrich, 1992; Whipple & Tucker, 1999). A fundamental assumption allowing us to solve Equation 1 for gully incision into abandoned alluvial terraces is that the time-integrated depth of incision (Δz [L]) can be estimated as the elevation difference between the gully bed and the elevation of the flat desert pavement surface above the gully (Supporting Information S1), as the latter effectively preserves the initial, pre-incision topography of the terrace (Figure 3).

For inversion of Equation 1 to infer incision rates for offset gullies a–c across the fault, the variables A and S can be measured directly from the DEM. However, model constants K, m, and n need to be a-priori known or alternatively locally determined. To locally calibrate model coefficients K, m, and n specifically for incision of the T3 terrace we applied Equation 1 for the lower-most section (outlet) of eight small tributaries that drain $T3_E$

into its eastern bounding channel (Figure 3). We assume that the tributaries and gullies on $T3_E$ evolved through the incision process described by Equation 1, that drainage area remained constant through time (e.g., Barnhart et al., 2020; Fox et al., 2014; Goren, Fox, et al., 2014), that incision started shortly after T3 was abandoned and that tributaries' outlet profiles "instantaneously" adjust (i.e., are in topographic steady state) to a constant base-level lowering-rate dictated by the bounding channel. Under these assumptions, the left hand side of Equation 1 can be computed for each tributary from the abandonment age of $T3_E$ (Δt) and the elevation difference (Δz) between a tributary outlet and the adjacent flat terrace surface. Thus, measuring Δz, A, and S for each tributary outlet using the DEM yielded an overdetermined system of eight equations and three unknowns, that is, K, m, and n. We solved this system and estimated the associated uncertainties through a combination of least squares regression and Monte Carlo simulations (Supporting Information S1).

After solving locally for K, m, and n, Equation 2 can be reorganized to calculate the timing of across-fault incision for gullies a–c (Δt_{AF}):

$$\Delta t_{AF} = \Delta z / K' A^{m'} S^{n'} \quad (2)$$

where (') denotes the locally calibrated model coefficients for fluvial incision into $T3_E$, and Δz, A, and S were measured for each offset gully over a segment located directly above the fault line (Figure 3). We note that the base-level lowering rate for the offset gullies above the fault is effectively set by the fault motion together with the incision of the gully section downstream from the fault. We found that across-fault incision of gullies a, b, and c was asynchronous and occurred at 0.83 ± 0.22, 0.31 ± 0.05, and 0.26 ± 0.06 the age of T3 abandonment, respectively (Figure 4a). Slip-rates inferred by dividing the offset of gullies a, b, and c (i.e., 20, 9, 8 m, respectively) by these relative geomorphic across-fault incision ages all fall within measurement uncertainty of the slip-rate recorded by $T3_W$ and its 28 m of sinistral offset (Figure 4b). Thus, regardless of the actual age of T3—our results imply an approximately constant lateral slip-rate for the Chijin segment of the ATF since T3 abandonment.

Assuming the luminescence age of 52 ± 4 ka for T3 abandonment yields across-fault incision ages of 43 ± 11, 16 ± 3, and 14 ± 3 ka for gullies a, b, and c, respectively, which translate to respective horizontal slip-rates of 0.47 ± 0.13, 0.57 ± 0.16, and 0.59 ± 0.20 mm/yr (Figure 4b). The magnitude of these late Quaternary geologic slip-rates is consistent with the <1 mm/yr GPS velocities previously reported for this Yumen segment of the ATF (Li et al., 2018).

5. Discussion

Geomorphic across-fault incision ages computed for offset gullies a–c (Figure 4) meet the following set of "sanity check" criteria: (a) larger gully offsets correspond to older across-fault incision ages; (b) across-fault incision ages should be (and are) less than or equal to the age of the T3 surface they incise; (c) both the m/n ratio and the reference K value (computed with commonly used m and n values: $m = 0.4$, $n = 1$, e.g. (Hilley et al., 2019; Stock & Montgomery, 1999), we obtained during calibration, that is, 0.62 ± 0.01 and $7.8 \pm 0.4 \times 10^{-5}$ [$yr^{-1}\,m^{0.2}$], respectively, are within the range of values typically reported in applications of the stream-power law, that is, 0.35–0.7 for m/n and 10^{-2}–10^{-7} [$yr^{-1}\,m^{0.2}$] for K (Harel et al., 2016; Hilley et al., 2019; Stock & Montgomery, 1999); (d) The slip-rates of ~0.5 mm/yr inferred from the geomorphic incision ages at the Chijin site (Figure 4) are geologically consistent with the expected eastwards decrease of the ATF's slip-rates from 1 to 2 mm/yr at the Hongliugou site located 10 km to the west (Xu, 2005; Zhang et al., 2007) to zero at the faults termination ~15 km to the east (Figure 2).

Nonetheless, application of model-based dating of gully incision is not devoid of limitations as it hinges on the validity of fundamental assumptions commonly employed to simplify complex natural settings. For example, the assumption that A does not change significantly during channel evolution (Barnhart et al., 2020; Fox et al., 2014; Goren, Willett, et al., 2014) may not necessarily hold for all gullies on the $T3_E$ terrace (Supporting Information S1). We, therefore, limited our analyses to gullies incising terrace sections where the preserved desert pavement surface suggests minimal drainage area reorganization (Abrahams & Parsons, 1991; Figure 3). We also note that while the relative simplicity of our geomorphic modeling approach is appealing as it facilitates geomorphic dating based on commonly used measures of gully profile geometry, its application relies on assumption of steady state profile at gully outlets, a constant base-level lowering and detachment limited channel erosion. Deviations from these assumptions may cause the somewhat low R^2 for the least squares regression used

to constrain the model parameters ($R^2 = 0.56$ [+0.009, −0.018], P-value = 0.03 [+0.005, −0.002], averaged over all Monte Carlo simulations, Supporting Information S1). Therefore, more complex models requiring calibration of a larger set of parameters (e.g., Barnhart et al., 2020; van der Beek & Bishop, 2003) may help extend model-based dating of incision to other settings with more complex geomorphic scenarios where, for example, gullies can transition from detachment to transport limited conditions, have a threshold shear stress for erosion, and/or experience temporally variable base-level lowering rates. Nonetheless, it appears that the relatively simple modeling approach employed at the Chijin site yielded dating results that were consistent with the aforementioned set of sanity check criteria.

Luminescence dating and geomorphic modeling of gully incision indicate that propagation of the ATF eastwards beyond the Chijin site occurred prior to 176 ka and that sinistral deformation across this segment of the ATF reached a constant rate of 0.5–0.6 mm/yr by at least 52 ka (Figure 4). Thus, it appears that most of the Pleistocene acceleration in slip across the ATF's juvenile Yumen segment (i.e., from zero to the present-day rate of 0.5 ± 0.1 mm/yr) predated the late Quaternary. Prolonged periods of constant deformation rates near the ATF's termination, such as those measured herein at the Chijin site, may be more consistent with an episodic (stepwise) rather than a continuous (gradual) shear propagation model for the Tibetan plateau. However, the uncertainty in the late Quaternary slip-rates obtained herein and the loose age constraints available for initiation of Pleistocene slip at the Chijin site preclude unequivocal distinction between these two shear propagation models. Thus, longer-term Pleistocene slip-rate measurements combined with the constant late Quaternary slip determined herein may ultimately help distinguish between episodic vs. gradual Pleistocene slip-acceleration at the eastern termination of the ATF.

6. Conclusions

Geomorphic incision dating for three gullies that were differentially offset across the Yumen segment of the ATF revealed asynchronous across-fault incision ages as much as threefold younger than the age of the alluvial strata they incise. Calculated slip-rates based on this new dating technique are consistent with longer-term late Quaternary sinistral slip-rates that were obtained at the same site using offsets of terrace boundaries and luminescence dating for age control. All together our results indicate time-invariant sinistral slip of 0.5 ± 0.1 mm/yr across the Yumen segment of the ATF during the late Quaternary and bring us closer to distinguishing between episodic (stepwise) vs. continuous (gradual) expansion of the Tibetan plateau northeastwards into central Asia.

Conflict of Interest

The authors declare no conflicts of interest relevant to this study.

Data Availability Statement

The raw DEM data used for our topography analyses in this study were deposited into ZENODO database (https://zenodo.org/record/5717733#.YZtWTbqxU2w) and available under https://doi.org/10.5281/zenodo.5717733.

Acknowledgments
The authors thank two anonymous reviewers and the editors for insightful comments and suggestions that greatly improved the manuscript. This study was funded by joint Israel Science Foundation—National Science Foundation of China (ISF-NSFC) research grant # 2568/17 to HZ and AM.

References

Abrahams, A. D., & Parsons, A. J. (1991). Relation between infiltration and stone cover on a semiarid hillslope, southern Arizona. *Journal of Hydrology*, *122*(1), 49–59. https://doi.org/10.1016/0022-1694(91)90171-D

Allen, M. B., Walters, R. J., Song, S., Saville, C., Paola, N. D., Ford, J., et al. (2017). Partitioning of oblique convergence coupled to the fault locking behavior of fold-and-thrust belts: Evidence from the Qilian Shan, northeastern Tibetan Plateau. *Tectonics*, *36*(9), 1679–1698. https://doi.org/10.1002/2017TC004476

Andrews, D. J., & Hanks, T. C. (1985). Scarp degraded by linear diffusion: Inverse solution for age. *Journal of Geophysical Research: Solid Earth*, *90*(B12), 10193–10208. https://doi.org/10.1029/JB090iB12p10193

Barnhart, K. R., Tucker, G. E., Doty, S., Shobe, C. M., Glade, R. C., Rossi, M. W., & Hill, M. C. (2020). Inverting topography for landscape evolution model process representation: Part 3. Determining parameter ranges for select mature geomorphic transport laws and connecting changes in fluvial erodibility to changes in climate. *Journal of Geophysical Research: Earth Surface*, *125*(7), e2019JF005287. https://doi.org/10.1029/2019JF005287

Bennett, R. A., Friedrich, A. M., & Furlong, K. P. (2004). Codependent histories of the San Andreas and San Jacinto fault zones from inversion of fault displacement rates. *Geology*, *32*(11), 961–964. https://doi.org/10.1130/G20806.1

Burbank, D. W., & Anderson, R. S. (2011). *Tectonic geomorphology*. John Wiley & Sons.

Chen, Y., Li, S.-H., & Li, B. (2012). Slip-rate of the Aksay segment of Altyn Tagh Fault revealed by OSL dating of river terraces. *Quaternary Geochronology*, *10*, 291–299. https://doi.org/10.1016/j.quageo.2012.04.012

Cowgill, E. (2007). Impact of riser reconstructions on estimation of secular variation in rates of strike-slip faulting: Revisiting the Cherchen River site along the Altyn Tagh Fault, NW China. *Earth and Planetary Science Letters*, *254*(3–4), 239–255. https://doi.org/10.1016/j.epsl.2006.09.015

Cowgill, E., Gold, R. D., Xuanhua, C., Xiao-Feng, W., Arrowsmith, J. R., & Southon, J. (2009). Low Quaternary slip-rate reconciles geodetic and geologic rates along the Altyn Tagh Fault, northwestern Tibet. *Geology*, *37*(7), 647–650. https://doi.org/10.1130/G25623A.1

D'Arcy, M., Schildgen, T. F., Turowski, J. M., & DiNezio, P. (2019). Inferring the timing of abandonment of aggraded alluvial surfaces dated with cosmogenic nuclides. *Earth Surface Dynamics*, *7*(3), 755–771. https://doi.org/10.5194/esurf-7-755-2019

Dietrich, W. E., Bellugi, D. G., Sklar, L. S., Stock, J. D., Heimsath, A. M., & Roering, J. J. (2003). Geomorphic transport laws for predicting landscape form and dynamics. In P. R.Wilcock, & R. M.Iverson (Eds.), *Geophysical Monograph Series* (pp. 103–132). American Geophysical Union. https://doi.org/10.1029/135GM09

Dolan, J. F., McAuliffe, L. J., Rhodes, E. J., McGill, S. F., & Zinke, R. (2016). Extreme multi-millennial slip-rate variations on the Garlock fault, California: Strain super-cycles, potentially time-variable fault strength, and implications for system-level earthquake occurrence. *Earth and Planetary Science Letters*, *446*, 123–136. https://doi.org/10.1016/j.epsl.2016.04.011

Duvall, A. R., & Tucker, G. E. (2015). Dynamic ridges and valleys in a strike-slip environment: Strike-slip landscapes. *Journal of Geophysical Research: Earth Surface*, *120*(10), 2016–2026. https://doi.org/10.1002/2015JF003618

Elliott, A. J., Oskin, M. E., Liu-Zeng, J., & Shao, Y. (2015). Rupture termination at restraining bends: The last great earthquake on the Altyn Tagh Fault. *Geophysical Research Letters*, *42*(7), 2164–2170. https://doi.org/10.1002/2015GL063107

Enzel, Y., Amit, R., Porat, N., Zilberman, E., & Harrison, B. J. (1996). Estimating the ages of fault scarps in the Arava, Israel. *Tectonophysics*, *253*(3–4), 305–317. https://doi.org/10.1016/0040-1951(95)00072-0

Faershtein, G., Porat, N., Avni, Y., & Matmon, A. (2016). Aggradation-incision transition in arid environments at the end of the Pleistocene: An example from the Negev Highlands, southern Israel. *Geomorphology*, *253*, 289–304. https://doi.org/10.1016/j.geomorph.2015.10.017

Fox, M., Goren, L., May, D. A., & Willett, S. D. (2014). Inversion of fluvial channels for paleorock uplift rates in Taiwan. *Journal of Geophysical Research: Earth Surface*, *119*(9), 1853–1875. https://doi.org/10.1002/2014JF003196

Frankel, K. L., & Dolan, J. F. (2007). Characterizing arid region alluvial fan surface roughness with airborne laser swath mapping digital topographic data. *Journal of Geophysical Research: Earth Surface*, *112*(F2). https://doi.org/10.1029/2006JF000644

Galbraith, R. F., Roberts, R. G., Laslett, G. M., Yoshida, H., & Olley, J. M. (1999). Optical dating of single and multiple grains of quartz from Jinmium rock shelter, northern Australia: Part I. Experimental design and statistical models. *Archaeometry*, *41*(2), 339–364. https://doi.org/10.1111/j.1475-4754.1999.tb00987.x

Gold, R. D., Cowgill, E., Arrowsmith, J. R., Chen, X., Sharp, W. D., Cooper, K. M., & Wang, X.-F. (2011). Faulted terrace risers place new constraints on the late Quaternary slip-rate for the central Altyn Tagh Fault, northwest Tibet. *GSA Bulletin*, *123*(5–6), 958–978. https://doi.org/10.1130/B30207.1

Gold, R. D., Cowgill, E., Arrowsmith, J. R., & Friedrich, A. M. (2017). Pulsed strain release on the Altyn Tagh Fault, northwest China. *Earth and Planetary Science Letters*, *459*, 291–300. https://doi.org/10.1016/j.epsl.2016.11.024

Gold, R. D., Cowgill, E., Arrowsmith, J. R., Gosse, J., Chen, X., & Wang, X. (2009). Riser diachroneity, lateral erosion, and uncertainty in rates of strike-slip faulting: A case study from Tuzidun along the Altyn Tagh Fault, NW China. *Journal of Geophysical Research*, *114*(B4). https://doi.org/10.1029/2008JB005913

Goren, L., Fox, M., & Willett, S. D. (2014). Tectonics from fluvial topography using formal linear inversion: Theory and applications to the Inyo Mountains, California. *Journal of Geophysical Research: Earth Surface*, *119*(8), 1651–1681. https://doi.org/10.1002/2014JF003079

Goren, L., Willett, S. D., Herman, F., & Braun, J. (2014). Coupled numerical-analytical approach to landscape evolution modeling. *Earth Surface Processes and Landforms*, *39*(4), 522–545. https://doi.org/10.1002/esp.3514

Harel, M.-A., Mudd, S. M., & Attal, M. (2016). Global analysis of the stream-power law parameters based on worldwide ^{10}Be denudation rates. *Geomorphology*, *268*, 184–196. https://doi.org/10.1016/j.geomorph.2016.05.035

Harkins, N., & Kirby, E. (2008). Fluvial terrace riser degradation and determination of slip-rates on strike-slip faults: An example from the Kunlun fault, China. *Geophysical Research Letters*, *35*(5), L05406. https://doi.org/10.1029/2007GL033073

He, J., Vernant, P., Chéry, J., Wang, W., Lu, S., Ku, W., et al. (2013). Nailing down the slip-rate of the Altyn Tagh Fault. *Geophysical Research Letters*, *40*(20), 5382–5386. https://doi.org/10.1002/2013GL057497

Hetzel, R. (2013). Active faulting, mountain growth, and erosion at the margins of the Tibetan Plateau constrained by in situ-produced cosmogenic nuclides. *Tectonophysics*, *582*, 1–24. https://doi.org/10.1016/j.tecto.2012.10.027

Hetzel, R., Niedermann, S., Tao, M., Kubik, P. W., Ivy-Ochs, S., Gao, B., & Strecker, M. R. (2002). Low slip-rates and long-term preservation of geomorphic features in Central Asia. *Nature*, *417*(6887), 428–432. https://doi.org/10.1038/417428a

Hilley, G. E., DeLong, S., Prentice, C., Blisniuk, K., & Arrowsmith, J. R. (2010). Morphologic dating of fault scarps using airborne laser swath mapping (ALSM) data: Scarp dating for the 21st century. *Geophysical Research Letters*, *37*(4). https://doi.org/10.1029/2009GL042044

Hilley, G. E., Porder, S., Aron, F., Baden, C. W., Johnstone, S. A., Liu, F., et al. (2019). Earth's topographic relief potentially limited by an upper bound on channel steepness. *Nature Geoscience*, *12*(10), 828–832. https://doi.org/10.1038/s41561-019-0442-3

Howard, A. D. (1994). A detachment-limited model of drainage basin evolution. *Water Resources Research*, *30*(7), 2261–2285. https://doi.org/10.1029/94wr00757

Howard, A. D., & Kerby, G. (1983). Channel changes in badlands. *GSA Bulletin*, *94*(6), 739–752. https://doi.org/10.1130/0016-7606(1983)94<739:ccib>2.0.co;2;2

Hsu, L., & Pelletier, J. D. (2004). Correlation and dating of Quaternary alluvial-fan surfaces using scarp diffusion. *Geomorphology*, *60*(3–4), 319–335. https://doi.org/10.1016/j.geomorph.2003.08.007

Jiang, X.-D., & Li, Z.-X. (2014). Seismic reflection data support episodic and simultaneous growth of the Tibetan Plateau since 25 Myr. *Nature Communications*, *5*(1), 5453. https://doi.org/10.1038/ncomms6453

Kang, W., Xu, X., Oskin, M. E., Yu, G., Luo, J., Chen, G., et al. (2020). Characteristic slip distribution and earthquake recurrence along the eastern Altyn Tagh Fault revealed by high-resolution topographic data. *Geosphere*, *16*(1), 392–406. https://doi.org/10.1130/GES02116.1

Li, Y., Shan, X., Qu, C., Liu, Y., & Han, N. (2018). Crustal deformation of the Altyn Tagh Fault based on GPS. *Journal of Geophysical Research: Solid Earth*, *123*(11), 10309–10322. https://doi.org/10.1029/2018JB015814

Liang, S., Gan, W., Shen, C., Xiao, G., Liu, J., Chen, W., et al. (2013). Three-dimensional velocity field of present-day crustal motion of the Tibetan Plateau derived from GPS measurements. *Journal of Geophysical Research: Solid Earth*, *118*(10), 5722–5732. https://doi.org/10.1002/2013JB010503

Liu, J., Ren, Z., Zheng, W., Min, W., Li, Z., & Zheng, G. (2020). Late Quaternary slip-rate of the Aksay segment and its rapidly decreasing gradient along the Altyn Tagh Fault. *Geosphere*, *16*(6), 1538–1557. https://doi.org/10.1130/GES02250.1

Ludwig, L. G., Akçiz, S. O., Noriega, G. R., Zielke, O., & Arrowsmith, J. R. (2010). Climate-modulated channel incision and rupture history of the San Andreas Fault in the Carrizo plain. *Science*, *327*(5969), 1117–1119. https://doi.org/10.1126/science.1182837

Mériaux, A.-S., Tapponnier, P., Ryerson, F. J., Xiwei, X., King, G., Van der Woerd, J., et al. (2005). The Aksay segment of the northern Altyn Tagh Fault: Tectonic geomorphology, landscape evolution, and Holocene slip-rate. *Journal of Geophysical Research: Solid Earth*, *110*(B4). https://doi.org/10.1029/2004JB003210

Mériaux, A.-S., Van der Woerd, J., Tapponnier, P., Ryerson, F. J., Finkel, R. C., Lasserre, C., & Xu, X. (2012). The Pingding segment of the Altyn Tagh Fault (91°E): Holocene slip-rate determination from cosmogenic radionuclide dating of offset fluvial terraces. *Journal of Geophysical Research: Solid Earth*, *117*(B9), B09406. https://doi.org/10.1029/2012JB009289

Meyer, B., Tapponnier, P., Gaudemer, Y., Peltzer, G., Shunmin, G., & Zhitai, C. (1996). Rate of left-lateral movement along the easternmost segment of the Altyn Tagh Fault, east of 96°E (China). *Geophysical Journal International*, *124*(1), 29–44. https://doi.org/10.1111/j.1365-246X.1996.tb06350.x

Molnar, P., & Dayem, K. E. (2010). Major intracontinental strike-slip faults and contrasts in lithospheric strength. *Geosphere*, *6*(4), 444–467. https://doi.org/10.1130/GES00519.1

Murray, A. S., & Wintle, A. G. (2000). Luminescence dating of quartz using an improved single-aliquot regenerative-dose protocol. *Radiation Measurements*, *32*(1), 57–73. https://doi.org/10.1016/S1350-4487(99)00253-X

Peltzer, G., Tapponnier, P., & Armijo, R. (1989). Magnitude of late Quaternary left-lateral displacements along the north edge of Tibet. *Science*, *246*(4935), 1285–1289. https://doi.org/10.1126/science.246.4935.1285

Prescott, J. R., & Hutton, J. T. (1994). Cosmic ray contributions to dose rates for luminescence and ESR dating: Large depths and long-term time variations. *Radiation Measurements*, *23*(2), 497–500. https://doi.org/10.1016/1350-4487(94)90086-8

Reitman, N. G., Mueller, K. J., Tucker, G. E., Gold, R. D., Briggs, R. W., & Barnhart, K. R. (2019). Offset channels may not accurately record strike-slip fault displacement: Evidence from landscape evolution models. *Journal of Geophysical Research: Solid Earth*, *124*(12), 13427–13451. https://doi.org/10.1029/2019JB018596

Seidl, M., & Dietrich, W. E. (1992). The problem of channel erosion into bedrock. *Catena Supplement*, 23, 101–124.

Stock, J. D., & Montgomery, D. R. (1999). Geologic constraints on bedrock river incision using the stream-power law. *Journal of Geophysical Research: Solid Earth*, *104*(B3), 4983–4993. https://doi.org/10.1029/98JB02139

Su, Q., Yuan, D., Zhang, H., Manopkawee, P., Zhan, Y., Zhang, P., & Xie, H. (2019). Geomorphic evidence for northeastward expansion of the eastern Qilian Shan, northeastern Tibetan Plateau. *Journal of Asian Earth Sciences*, *177*, 314–323. https://doi.org/10.1016/j.jseaes.2019.04.003

Tapponnier, P., & Molnar, P. (1977). Active faulting and tectonics in China. *Journal of Geophysical Research*, *82*(20), 2905–2930. https://doi.org/10.1029/JB082i020p02905

Tapponnier, P., Zhiqin, X., Roger, F., Meyer, B., Arnaud, N., Wittlinger, G., & Jingsui, Y. (2001). Oblique stepwise rise and growth of the Tibet Plateau. *Science*, *294*(5547), 1671–1677. https://doi.org/10.1126/science.105978

van der Beek, P., & Bishop, P. (2003). Cenozoic river profile development in the Upper Lachlan catchment (SE Australia) as a test of quantitative fluvial incision models. *Journal of Geophysical Research: Solid Earth*, *108*(B6). https://doi.org/10.1029/2002JB002125

Wang, W., Zhang, P., Pang, J., Garzione, C., Zhang, H., Liu, C., et al. (2016). The Cenozoic growth of the Qilian Shan in the northeastern Tibetan Plateau: A sedimentary archive from the Jiuxi Basin. *Journal of Geophysical Research: Solid Earth*, *121*(4), 2235–2257. https://doi.org/10.1002/2015JB012689

Washburn, Z., Arrowsmith, J. R., Forman, S. L., Cowgill, E., Xiaofeng, W., Yueqiao, Z., & Zhengle, C. (2001). Late Holocene earthquake history of the central Altyn Tagh Fault, China. *Geology*, *29*(11), 1051–1054. https://doi.org/10.1130/0091-7613(2001)029<1051:LHEHOT>2.0.CO;2

Wesnousky, S. G. (2006). Predicting the endpoints of earthquake ruptures. *Nature*, *444*(7117), 358–360. https://doi.org/10.1038/nature05275

Whipple, K. X., & Tucker, G. E. (1999). Dynamics of the stream-power river incision model: Implications for height limits of mountain ranges, landscape response timescales, and research needs. *Journal of Geophysical Research: Solid Earth*, *104*(B8), 17661–17674. https://doi.org/10.1029/1999JB900120

Xiao, Q., Shao, G., Liu-Zeng, J., Oskin, M. E., Zhang, J., Zhao, G., & Wang, J. (2015). Eastern termination of the Altyn Tagh Fault, western China: Constraints from a magnetotelluric survey: Termination of the Altyn Tagh Fault. *Journal of Geophysical Research: Solid Earth*, *120*(5), 2838–2858. https://doi.org/10.1002/2014JB011363

Xu, X., Wang, F., Zheng, R., Chen, W., Ma, W., Yu, G., et al. (2005). Late Quaternary sinistral slip-rate along the Altyn Tagh. *Science in China Series D Earth Sciences*, *48*(3), 384. https://doi.org/10.1360/02yd0436

Xu, X., Zheng, F., & Wilson, G. V. (2021). Flow hydraulics in an ephemeral gully system under different slope gradients, rainfall intensities, and inflow conditions. *CATENA*, *203*, 105359. https://doi.org/10.1016/j.catena.2021.105359

Yin, A., Rumelhart, P. E., Butler, R., Cowgill, E., Harrison, T. M., Foster, D. A., et al. (2002). *Tectonic history of the Altyn Tagh Fault system in northern Tibet inferred from Cenozoic sedimentation* (Vol. 39). Geological Society of America Bulletin.

Zechar, J. D., & Frankel, K. L. (2009). Incorporating and reporting uncertainties in fault slip-rates. *Journal of Geophysical Research: Solid Earth*, *114*(B12). https://doi.org/10.1029/2009JB006325

Zhang, J., Yun, L., Zhang, B., Qu, J., Zhao, H., Hui, J., et al. (2020). Deformation at the easternmost Altyn Tagh Fault: Constraints on the growth of the northern Qinghai-Tibetan Plateau. *Acta Geologica Sinica—English Edition*, *94*(4), 988–1006. https://doi.org/10.1111/1755-6724.14555

Zhang, P.-Z., Molnar, P., & Xu, X. (2007). Late Quaternary and present-day rates of slip along the Altyn Tagh Fault, northern margin of the Tibetan Plateau. *Tectonics*, *26*(5). https://doi.org/10.1029/2006TC002014

Zhang, P.-Z., Shen, Z., Wang, M., Gan, W., Bürgmann, R., Molnar, P., et al. (2004). Continuous deformation of the Tibetan Plateau from global positioning system data. *Geology*, *32*(9), 809. https://doi.org/10.1130/G20554.1

Zheng, W., Zhang, P., He, W., Yuan, D., Shao, Y., Zheng, D., et al. (2013). Transformation of displacement between strike-slip and crustal shortening in the northern margin of the Tibetan Plateau: Evidence from decadal GPS measurements and late Quaternary slip-rates on faults. *Tectonophysics*, *584*, 267–280. https://doi.org/10.1016/j.tecto.2012.01.006

Zielke, O., Klinger, Y., & Arrowsmith, J. R. (2015). Fault slip and earthquake recurrence along strike-slip faults—Contributions of high-resolution geomorphic data. *Tectonophysics*, *638*, 43–62. https://doi.org/10.1016/j.tecto.2014.11.004

References From the Supporting Information

Aiken, S. J., & Brierley, G. J. (2013). Analysis of longitudinal profiles along the eastern margin of the Qinghai-Tibetan Plateau. *Journal of Mountain Science*, *10*(4), 643–657. https://doi.org/10.1007/s11629-013-2814-2

Lague, D. (2014). The stream-power river incision model: Evidence, theory, and beyond. *Earth Surface Processes and Landforms*, *39*(1), 38–61. https://doi.org/10.1002/esp.3462

Lin, A., Guo, J., Kano, K., & Awata, Y. (2006). Average slip rate and recurrence interval of large-magnitude earthquakes on the western segment of the strike-slip Kunlun fault, northern Tibet. *Bulletin of the Seismological Society of America*, *96*(5), 1597–1611. https://doi.org/10.1785/0120050051